HHS Public Access

Author manuscript

Nanomedicine. Author manuscript; available in PMC 2021 August 01.

Published in final edited form as:

Nanomedicine. 2020 August ; 28: 102205. doi:10.1016/j.nano.2020.102205.

Inhibition of Choroidal Neovascularization by Systemic Delivery of Gold Nanoparticles

Rupesh Singh, PhD[1,*], **Julia C. Batoki, A.A.S.**[1], **Mariya Ali, B.A.**[1], **Vera L. Bonilha, PhD**[1,2,3], **Bela Anand-Apte, MBBS, PhD**[1,2,3]

[1]Cole Eye Institute, Cleveland Clinic Foundation, Cleveland, OH

[2]Lerner Research Institute, Cleveland Clinic Foundation, Cleveland, OH

[3]Cleveland Clinic Lerner College of Medicine at Case Western Reserve University, Department of Ophthalmology and Molecular Medicine, Cleveland, OH

Abstract

Choroidal neovascularization (CNV) is the abnormal growth of blood vessels that sprout from the choroid vasculature and grow beneath and into the retina. The newly formed blood vessels in CNV often leak blood and fluid which deteriorates vision over time, eventually leading to blindness. In the present study, we examined the efficacy of intravenously injected gold nanoparticles in the laser-induced CNV animal model. Using optical coherence tomography (OCT) and fluorescein angiography, we evaluated CNV lesions longitudinally, over a period of 21 days, with and without nanoparticle treatment. Intravenously injected low concentration of bare gold nanoparticles showed significant anti-angiogenic properties by suppressing CNV development and progression. The treatment group showed significantly decreased fluorescein leakage at the CNV site compared to vehicle injected control mice. OCT assisted CNV volume measurement at all time points showed a significant reduction in lesion size in the treatment group compared with controls.

Graphical Abstract

The graphical abstract figure shows an experimental plan of treating laser induced CNV mouse models with intravenous gold nanoparticle (or sham PBS) with a follow-up scheme of in-vivo imaging. Also included are representative images of fluorescein angiography and optical coherence tomography scans of AuNP treated and control (sham) eyes.

[*]Corresponding author: [1]Cole Eye Institute, Cleveland Clinic Foundation, Cleveland, OH - 44195, USA. singhr4@ccf.org.

Author contributions: Conceptualization – RS, BA-A,; Data curation and Formal analysis – RS, JCB; Funding acquisition – BA-A; Investigation – JCB, RS; Methodology – JCB, VB, MA, RS; Resources – VB, MA; Software - RS; Roles/Writing - original draft - RS; Writing - review & editing – BA-A, JCB, MA.

Background

Age-related macular degeneration (AMD), is the leading cause of vision loss among the elderly in the western hemisphere. The neovascular form of AMD, called wet-AMD (wAMD), is characterized by the presence of choroidal neovascularization (CNV). Much of this vision loss in wAMD is a consequence of CNV, the abnormal growth and leakage of blood vessels beneath and into the retina[1]. Laser induced CNV in pigmented wild-type mice (C57BL6/J) is the most commonly used animal model of wAMD[2]. Literature suggests a well-established timeline of progression of laser induced CNV lesions in pigmented mice[3]. The progression of CNV can be monitored using immunostaining of choroidal-RPE flat-mounts[4] or using *in vivo* imaging techniques such as optical coherence tomography (OCT) and/or fluorescein (FA) and indocyanine green (ICG) angiography using confocal scanning laser ophthalmoscope (cSLO)[3, 5, 6]. The advantages of using *in vivo* imaging for CNV assessment include the ability to perform longitudinal imaging of the same animal over a long period of time and to assess CNV lesion characteristics such as dye leakage, blue and infrared autofluorescence, and infrared/dark field imaging for scar tissue formation[7]. In addition, *in vivo* volumetric OCT imaging provides the ability to visualize the physical volume of CNV lesions and their progression[4].

Current clinical management of wAMD includes intraocular injections of anti-VEGF therapeutics and occasionally laser induced photocoagulation, thermal therapy, and photodynamic therapy[8]. The challenges with the laser-based treatment include treatment efficiency and collateral tissue damage. While anti VEGF therapeutics have been extremely beneficial for wAMD, this therapeutic modality faces unique challenges that include selective responsiveness and patient discomfort because of repeated sessions of intraocular injections, leading to non-compliance. Some recent studies suggest that the use of photothermal contrast agent may improve laser based treatment efficiency[9]. However, a major hindrance to such an approach is the issue of effective drug delivery to the retina. Recent advancements in nanomedicine provide several efficient drug delivery options including some via the systemic route[10]. One such nanoparticle, the gold nanoparticle (AuNP) has been reported to invade and reach deep layers of retina and choroidal space both via intraocular and intravenous injections[11]. AuNPs have also been reported to have anti-angiogenic and anti-tumor properties[12, 13]. The anti-angiogenic activity of gold nanoparticles (AuNP) depends on many factors such as size, shape, and surface properties (charge, functionalization etc.)[13]. Its efficiency depends on the bioavailability of AuNPs at the disease site, concentration, as well as its permeability and retention in and around the target cells. Mukherjee et al.[12] demonstrated that AuNP's prevent angiogenesis by inhibiting heparin binding angiogenic factors such as vascular endothelial growth factor (VEGF) and fibroblast growth factor (FGF)[14]. While a number of studies in nanomedicine focus on the application of nanoparticles as a therapy for cancer, very little work has been done on their therapeutic potential in retinal diseases such as CNV. Roh et. al. reported that intravitreal injection of 20 nm gold nanoparticles had anti-CNV effects as assessed by choroidal flat mount stained with endothelial marker Isolectin B4[15].

The present study, for the first time, examines the therapeutic effect of systemically delivered AuNPs in an animal model of CNV. Long term *in vivo* disease progression of

CNV lesions was evaluated by high-resolution OCT imaging as well as angiography (Fluorescein and Indocyanine green) using cSLO imaging. The AuNP's were plasmonic nanoparticles optimized for photothermal therapy providing a possibility of combined anti-angiogenic/photothermal treatment strategy. Intravenous injections of low concentration bare gold nanoparticles (AuNP) solution was tested for their ability to inhibit laser-induced CNV. We further validated our findings with choroidal flat mounts stained with endothelial cell markers for CNV lesion size assessment.

Methods

Animals:

Eighteen pigmented wild type mice (three month old, sex matched, C57BL6/J) were purchased from Jackson Laboratory (Bar Harbor, ME). All animal experimentation was conducted in accordance with protocols approved by the Cleveland Clinic Institutional Animal Care and Use Committee (IACUC) and conformed to the National Institutes of Health Guide for the Care and Use of Animals in Research and the ARVO Statement for the Use of Animals in Ophthalmic and Vision Research as well as the EU directive 2010/63/EU for animal experiments. All mice were housed in 10/14 dark/light conditions and were provided food and water ad libitum. CNV lesions were induced in all mice following laser injury using green argon laser as described previously[16–18]. These mice were subsequently split into two groups viz. sham treated control and AuNP treated experimental group.

Laser induced choroidal neovascularization:

Mice were anesthetized with 65-68 mg/Kg sodium pentobarbital delivered intra-peritoneally. 0.5% procaine solution was placed on the cornea for topical anesthesia. Following pupil dilation with 0.5% topical tropicamide/phenylephrine combination drops (Santen Pharmaceuticals, Osaka, Japan), four laser burn spots were targeted to the superior, superior-temporal, or superior-nasal quadrants of the fundus using a 532nm laser beam from a green solid-state laser (Iridex oculight 532nm) delivered using a slit lamp (Haag Streit SL 1000). Laser power of 240 mW, 50 mili-second pulse duration and 50 μm spot size was used for all lesions. Figure 1c–f shows a representative OCT b-scan and cSLO infrared reflectance images of both control and AuNP treated mice groups captured on day 0 immediately laser injury. Laser lesion size was fairly uniform and consistent in our hands.

Nanoparticles:

Citrate reduced gold nanoparticles were purchased from Nanopartz Inc. The nanoparticles were used at a concentration of 4.37×10^{10} nps/mL, which is typically lower than recommended for nanoparticle assisted thermal therapies. The average diameter of AuNP's was 50 nm. The supplier provided characterization certificate for surface plasmon resonance (SPR), optical density (OD), concentration, and mean size of nanoparticles. The absorption profile of the nanoparticles was obtained using a nanodrop 2000 spectrophotometer (Thermo Scientific Inc.) which matched the supplier provided characterization (results not presented for brevity). All nanoparticles were pre-sterilized for *in vivo* use and were supplied with pathogen free certificates. The nanoparticles and Phosphate-Buffered Saline (PBS) (Corning, Mediatech Inc., USA) was injected intravenously in corresponding groups via tail vein on

day 0 of laser injury. All experimental animals received re-injections on respective day four after first injection. The volume of the nanoparticle solution (as well as control PBS) injected was 50 μl at both time points of injection. The selection of these time points for nanoparticle injections was based on previous studies that determined that CNV lesions had peak angiogenic activities between day 4 and day 7 after laser injury[19]. The control groups received sham PBS intravenous injections of 50 μl on day 0 of laser injury.

Optical coherence tomography:

All control mice (which received sham PBS intravenous injections) and experimental mice (which received intravenous AuNP injections) were evaluated longitudinally using *in vivo* imaging. Ultra high-resolution spectral domain optical coherence tomography (OCT) system (Envisu R2210 UHR Leica Microsystems Inc.) was used for *in vivo* cross-sectional imaging. Each animal was pre-imaged with a 55° mouse lens for pre-existing retinal anomalies and retinal structural integrity. The scan parameters used were 1.8 mm x 1.8 mm rectangular volume scan, 1000 a-scans / 200 b-scans averaged 3 times per b-scan. Immediately after the laser injury, each animal was scanned for ruptured Bruch's membrane as a checkpoint for successful CNV induction. The inclusion criteria to include a lesion in the quantitative analysis is described in Table 1. Each CNV lesion was then followed over time using the same scan parameters at day 7, 14, and 21. The volume of each lesion was calculated with OCT volumetric scans using previously described methods[20]. By assuming CNV lesion as an ellipsoid, volumes were obtained by measuring length, depth, and width of each lesion in OCT rectangular volumetric scans as described[20]. The B-scan was used to measure the width (a) and depth (b) of the lesion. The volume intensity projection image was used to measure the length (c) of the lesion. The lesion volume was calculated using the formula $A = \frac{4}{3}\pi abc$. The results on OCT based CNV volume were then compared for both experimental and control groups.

Scanning laser ophthalmoscopy:

Before the start of experiment, all the animals were imaged with cSLO (Heidelberg SPECTRALIS, Heidelberg Engineering, Germany) for any pre-existing abnormalities in the mouse retina. For all pre-screening and post laser imaging, the cSLO imaging modes used were infrared reflectance, red free dark field, visible (blue-green) autofluorescence, and infrared autofluorescence at both RPE-Choroid interface and vitreous-retina interface (not presented for brevity). In addition to these modes, in all post laser imaging, fluorescein angiography (FA) was performed at the RPE-choroid interface and vitreous-retina interface for early phase and late phase CNV leakage analysis. For intraperitoneally injected Na Fluorescein (1% in saline, 50 μl) (AL-FLUOR 10%, Akron Inc.) early phase images of fluorescein angiography (FA) were taken at ~3 mins and late phase images were taken at ~6 mins. The leakage area was measured with inbuilt analysis software of Heidelberg Spectralis imaging system. In high-resolution mode, the system provides an image pixel format of 1536 x 1536 with the wide-field lens. CNV images were analyzed in ImageJ (Version 1.52a) by measuring area of leakage. This value was then normalized for size of laser burn measured at day 3 in IRDF images.

Immunohistochemistry:

Following day 21 cSLO and OCT retinal and fundus scans, animals were humanely euthanized using a cocktail of ketamine (90 mg/ml, ketamine HCL, Zoetis) and xylazine (10 mg/ml, AnaSed Injection) injection followed by cervical dislocation. Eyes were then enucleated and placed directly into 4% PFA (Electron Microscopy Sciences) overnight at 4°C with an incision along with limbus to allow for infiltration of the fixative. Choroid was isolated by dissecting and removing both the anterior chamber and retina. Samples were post-fixed in pure methanol for 10 minutes in −20°C, then placed in perm/block buffer with concentration of: 1% BSA (Fisher Bioreagents), 1X PBS, and 0.1% Triton (Bio-Rad Laboratories, Inc.) overnight at 4°C on a shaker. Samples were stained with Isolectin 488 (Invitrogen, Thermo Fisher Scientific) in perm/block for 2 days (1:50), washed 3 times with 1X PBS, and flat mounted under light microscope and sealed. Slides were observed under a confocal microscope (Leica microsystem) using a 488 nm green laser. Images were analyzed for quantification of CNV lesion area and intensity. A previously published background correction method, total corrected cellular fluorescence (TCCF)[21], was used to quantify the total lesion area with background corrected autofluorescence.

Transmission electron microscopy:

On day 4 of laser injury, mice were euthanized as described above at 1-hour post-injection. Eyes were enucleated and placed in 2% PFA and 2.5% glutaraldehyde (Polysciences, Inc.) in 0.1 M sodium cacodylate buffer (pH 7.3) (Sigma-Aldrich) with 5mM $CaCl_2$. Under a dissecting microscope, anterior segments were removed. Eyecups with the retina exposed were then washed in three changes of 0.1 M sodium cacodylate buffer for fifteen minutes each and post-fixed in 1% OsO4 (Electron Microscopy Sciences) in 0.1 M sodium cacodylate buffer for 45 minutes at 4°C. Finally, the tissues were washed in two changes of 0.1 M cacodylate buffer and left in wash overnight at 4°C. Following, each sample was sequentially incubated in increasing percentages of ethanol (35%, 50%, 75%, 85%, 95%, and 100%) for 15 minutes at 4°C. Samples were incubated in 1:1 100% ethanol and propylene oxide (Fisher Scientific) and 100% propylene oxide for fifteen minutes each, followed by an immersion of 2:1 propylene oxide and epon resin for 30 minutes each on rotisserie with caps, and 1:1 propylene oxide and epon for 3 hours with the caps. Caps were removed, eyes were incubated and infiltrated overnight in epon resin. Next day, eyes were embedded into mold with fresh resin. Samples were polymerized at 60°C for three days. The tissue was cut into thin sections (~1 μm) with a diamond knife and stained with toluidine blue (Fisher Chemical) dye. The TEM images were acquired using Tecnai G2 Spirit BioTWIN electron microscope operated at 80 kV.

Statistics:

For all measurements of FA leakage area and OCT lesion volume, and choroidal flat-mount TCCF between treatment and control group, a two-tailed non-parametric student t-test was performed using GraphPad Prism version 8.1.1 for Windows (GraphPad Software, San Diego, California USA). The accepted value for rejecting the null was set at $P < 0.05$ with confidence interval of 95%. All data are presented in the form of mean with the standard error of the mean (SEM).

Results

Fluorescein angiography:

The areas of dye leakage of Na fluorescein were measured from images obtained on days 7, 14, and 21 post laser injury, and were compared for statistical differences between AuNP treated and sham treated groups. Size of laser lesions (SLO images at day 0) were similar between all groups. Figure 2 shows two sets of representative FA images for each sham group (a-b) and AuNP treatment group (c-d). A significantly reduced area of leakage was observed in the AuNP treatment group (Fig. 2 (c–d)) at all three time points compared with the sham group (Fig. 2 (a–b)). Statistical analysis showed that these changes were statistically significant at all time points evaluated (Fig. 3). For the early phase FA, on average, the dye leakage area was decreased in the treatment group by 29% on day 7, 42% on day 14, and 48% on day 21. For late phase FA, the percentage decrease in treatment group was 37% on day 7, 44% on day 14, and 48 % on day 21. In order to assess the extent and severity of FA leakage in both groups, a difference in the late phase and early phase FA was obtained and compared (Fig. 3c). The average percent decrease in FA difference (FA difference = FA late − FA early) for the treatment group was 57% on day 7, 48 % on day 14 and 46 % on day 21.

OCT Lesion Volume:

The CNV lesion volume in control and experimental groups were compared at all imaging time points, viz; day 7, 14, and 21. Representative comparison of OCT B-scans of sham treated mice (Fig. 4a) and AuNP treated mice (Fig. 4b) show reduced CNV lesion size in AuNP treated mice. Quantitation of CNV lesion volumes showed a statistically significant decrease in AuNP treated mice at all time points evaluated (Fig. 4c), with ~ 53% decrease on day 7 and 14, and −35% decrease on day 21. Laser-induced CNV in pigmented mice undergoes spontaneous healing after two weeks resulting in a decrease in the overall lesion volume in both groups by day 21 (Fig. 4c).

Immunohistochemistry and TEM:

CNV lesion area was also calculated from retinal flat mounts stained with Isolectin B4 (an endothelial cell marker) as shown in Fig. 5a–b. Figure 5a is a representative image of a retinal flat mount from a sham control mouse while Fig. 5b is a representative flat mount from an AuNP treated mouse. There appears to be a decrease in the size of the CNV lesions in mice treated with AuNP, which corroborates the findings from in vivo analyses. Quantitation of CNV lesion area from retinal flat mounts were calculated in ImageJ[22] using TCCF[21], where TCCF = Integrated Density − (Area of selected cell X Mean fluorescence of background readings). Statistical analysis (Fig. 5c), showed a significant decrease (~75% decrease) in TCCF of AuNP treated mice compared with sham treated controls.

To evaluate if injected AuNPs reach the CNV lesion, transmission electron microscope (TEM) images of sections through the CNV lesion were evaluated (Fig. 6). Gold nanoparticles were seen at the CNV site (Fig. 6c) and RPE – photoreceptor junctions (Fig. 6d). It was also observed that few nanoparticles penetrated through the inner retinal layers such as outer nuclear layer and ganglion cell layer (results not presented).

Discussion

AuNPs have been shown to be effective as a therapeutic in a variety of disease models especially cancer[23–26]. The present study, demonstrates for the first time that intravenously injected AuNP's exhibit a robust anti-angiogenic and therapeutic effect for CNV in the laser-induced CNV mouse model. Previous *in vitro* studies have suggested that AuNPs mediate their anti-angiogenic effects by targeting the VEGFA/VEGFR pathway as well as by regulating inflammatory mediators[26, 27]. A few studies have shown that intravitreal administration of AuNPs have the ability to inhibit retinal neovascularization in animal models with minimal toxicity[27–29].

While prior experiments have determined that the cellular uptake and internalization of AuNPs are dependent on physical properties of the nanoparticle such as size, shape, charge and functionalization and occurs via receptor mediated endocytosis or phagocytosis, pinocytosis or passive uptake through the cell membrane, the mechanisms of uptake in the retina have not been examined. Using transmission electron microscopy, we found systemically delivered nanoparticles to be localized to the CNV lesion as well as in the retina. We hypothesize that the fenestrae in the choriocapillaris (~2-3 RBC wide) may allow for localization of AuNPs in the retina even in the presence of an intact blood retinal barrier[30, 31]. In a healthy retina, RPE tight junctions form the outer blood retinal barrier and prevents material from entering the retina. In pathological conditions, such as CNV in age-related macular degeneration, there is a disruption of the outer blood retinal barrier, which leads to damage to the photoreceptor cells. We hypothesize that this outer blood retinal barrier breakdown will likely play a role in the increased bioavailability of AuNP into and around the CNV lesions[32]. Additional studies identifying the molecular pathways that are involved in AuNP mediated inhibition of neovascularization are warranted. Whether targeting VEGF via these AuNP particles will have an additive effect is another area that could be explored.

That systemic administration of AuNPs can generate a strong therapeutic response without toxicity, similar in nature to that reported previously with intravitreal injections, suggests that this mode of delivery might be preferable in terms of patient compliance and intra-ocular complications associated with repeated intravitreal injections. Our protocol for longitudinal *in vivo* assessment of CNV progression provides insight into the anti-angiogenic therapeutic effects of gold nanoparticle in a temporal fashion. Similar studies may be used to guide treatment protocols in models of sustained CNV.

In this work, the gold nanoparticles used were intentionally made plasmonic for laying the foundation and demonstrating the feasibility of combined anti-angiogenic and laser photocoagulation therapeutic studies. In the future, we will identify AuNP modifications such as biocompatible coatings that might increase the AuNP bioavailability. AuNPs (bare and PEG coated) have been reported to have none or negligible toxicity *in vitro* and *in vivo*[11]. In the present study, we observed no visible signs of unexplained injury, inflammation, or any reflectivity change due to atrophy in any mouse. Future studies will include detailed toxicity analysis.

The treatment of choroidal and chorioretinal diseases using nanomedicine and nanotechnology assisted laser therapies have shown great promise for effective and efficient localized and selective drug delivery. This study is a first step towards that goal. Additional studies will require more systematic investigation for translation and clinical usefulness.

Acknowledgement:

The authors would like to thank the Imaging Core of Lerner Research Institute of Cleveland Clinic Foundation for their assistance with TEM imaging and the Biological Resource Unit (BRU) for their help with animal husbandry. This work was supported in part by US National Institute of Health EY027083 (BA-A), EY026181 (BA-A), P30EY025585(BA-A), EY027750 (VLB), Research to Prevent Blindness (RPB) Challenge Grant and RPB Lew Wasserman award to BA-A, Cleveland Eye Bank Foundation Grant and funds from Cleveland Clinic Foundation.

References:

1. Ambati J and Fowler BJ, Mechanisms of age-related macular degeneration. Neuron. 2012;75:26–39 [PubMed: 22794258]
2. Edwards AO and Malek G, Molecular genetics of AMD and current animal models. Angiogenesis. 2007;10:119–32 [PubMed: 17372852]
3. Gong Y, Li J, Sun Y, Fu Z, Liu C-H, Evans L, et al., Optimization of an Image-Guided Laser-Induced Choroidal Neovascularization Model in Mice. Plos One. 2015;10:e0132643–e0132643 [PubMed: 26161975]
4. Ragauskas S, Kielczewski E, Vance J, Kaja S and Kalesnykas G, In Vivo Multimodal Imaging and Analysis of Mouse Laser-Induced Choroidal Neovascularization Model. Journal of visualized experiments : JoVE. 2018
5. Nagai N, Lundh von Leithner P, Izumi-Nagai K, Hosking B, Chang B, Hurd R, et al., Spontaneous CNV in a novel mutant mouse is associated with early VEGF-A-driven angiogenesis and late-stage focal edema, neural cell loss, and dysfunction. Invest Ophthalmol Vis Sci. 2014;55:3709–19 [PubMed: 24845632]
6. Singh R, Batoki J and Anand-Apte B, 2019 Therapeutic response of experimental choroidal neovascularization in mice with photodynamic/photothermal therapy using ICG loaded gold nanorods as a photosensitizer 17th International Photodynamic Association World Congress,
7. Park JR, Choi W, Hong HK, Kim Y, Jun Park S, Hwang Y, et al., Imaging Laser-Induced Choroidal Neovascularization in the Rodent Retina Using Optical Coherence Tomography Angiography. Investigative Ophthalmology & Visual Science. 2016;57:OCT331–OCT340 [PubMed: 27409490]
8. Schmidt-Erfurth UM and Pruente C, Management of neovascular age-related macular degeneration. Progress in retinal and eye research. 2007;26:437–451 [PubMed: 17512238]
9. Farjo KM and Ma JX, The potential of nanomedicine therapies to treat neovascular disease in the retina. Journal of angiogenesis research. 2010;2:21 [PubMed: 20932321]
10. Jiang S, Franco YL, Zhou Y and Chen J, Nanotechnology in retinal drug delivery. Int J Ophthalmol. 2018;11:1038–1044 [PubMed: 29977820]
11. Kim JH, Kim JH, Kim KW, Kim MH and Yu YS, Intravenously administered gold nanoparticles pass through the blood-retinal barrier depending on the particle size, and induce no retinal toxicity. Nanotechnology. 2009;20:505101 [PubMed: 19923650]
12. Mukherjee P, Bhattacharya R, Wang P, Wang L, Basu S, Nagy JA, et al., Antiangiogenic properties of gold nanoparticles. Clin Cancer Res. 2005;11:3530–4 [PubMed: 15867256]
13. Arvizo RR, Rana S, Miranda OR, Bhattacharya R, Rotello VM and Mukherjee P, Mechanism of anti-angiogenic property of gold nanoparticles: role of nanoparticle size and surface charge. Nanomedicine. 2011;7:580–587 [PubMed: 21333757]
14. Arvizo RR, Rana S, Miranda OR, Bhattacharya R, Rotello VM and Mukherjee P, Mechanism of anti-angiogenic property of gold nanoparticles: role of nanoparticle size and surface charge. Nanomedicine. 2011;7:580–7 [PubMed: 21333757]

15. Roh Y-J, Rho CR, Cho W-K and Kang S, The Antiangiogenic Effects of Gold Nanoparticles on Experimental Choroidal Neovascularization in Mice. Investigative Ophthalmology & Visual Science. 2016;57:6561–6567 [PubMed: 27918830]
16. Ebrahem Q, Qi JH, Sugimoto M, Ali M, Sears JE, Cutler A, et al., Increased neovascularization in mice lacking tissue inhibitor of metalloproteinases-3. Investigative ophthalmology & visual science. 2011;52:6117–6123 [PubMed: 21282576]
17. Qi JH, Bell B, Singh R, Batoki J, Wolk A, Cutler A, et al., Sorsby Fundus Dystrophy Mutation in Tissue Inhibitor of Metalloproteinase 3 (TIMP3) promotes Choroidal Neovascularization via a Fibroblast Growth Factor-dependent Mechanism. Sci Rep. 2019;9:17429 [PubMed: 31757977]
18. Qi JH, Ebrahem Q, Ali M, Cutler A, Bell B, Prayson N, et al., Tissue inhibitor of metalloproteinases-3 peptides inhibit angiogenesis and choroidal neovascularization in mice. Plos One. 2013;8:e55667–e55667 [PubMed: 23469166]
19. Itaya M, Sakurai E, Nozaki M, Yamada K, Yamasaki S, Asai K, et al., Upregulation of VEGF in murine retina via monocyte recruitment after retinal scatter laser photocoagulation. Investigative Ophthalmology & Visual Science. 2007;48:5677–5683 [PubMed: 18055819]
20. Sulaiman RS, Quigley J, Qi X, O'Hare MN, Grant MB, Boulton ME, et al., A Simple Optical Coherence Tomography Quantification Method for Choroidal Neovascularization. J Ocul Pharmacol Ther. 2015;31:447–454 [PubMed: 26060878]
21. McCloy RA, Rogers S, Caldon CE, Lorca T, Castro A and Burgess A, Partial inhibition of Cdk1 in G2 phase overrides the SAC and decouples mitotic events. Cell Cycle. 2014;13:1400–1412 [PubMed: 24626186]
22. Rueden CT, Schindelin J, Hiner MC, DeZonia BE, Walter AE, Arena ET, et al., ImageJ2: ImageJ for the next generation of scientific image data. BMC Bioinformatics. 2017;18:529 [PubMed: 29187165]
23. Mukherjee P, Bhattacharya R, Wang P, Wang L, Basu S, Nagy JA, et al., Antiangiogenic properties of gold nanoparticles. Clin Cancer Res. 2005;11:3530–3534 [PubMed: 15867256]
24. Arvizo RR, Miranda OR, Bhattacharya R, Rotello VM and Mukherjee P, Antiangiogenic properties of gold nanoparticles: Effect of size and surface charge. Abstr Pap Am Chem S. 2010;240
25. Mukherjee S and Patra CR, Therapeutic application of anti-angiogenic nanomaterials in cancers. Nanoscale. 2016;8:12444–12470 [PubMed: 27067119]
26. Darweesh RS, Ayoub NM and Nazzal S, Gold nanoparticles and angiogenesis: molecular mechanisms and biomedical applications. Int J Nanomed. 2019;14:7643–7663
27. Kim JH, Kim MH, Jo DH, Yu YS, Lee TG and Kim JH, The inhibition of retinal neovascularization by gold nanoparticles via suppression of VEGFR-2 activation. Biomaterials. 2011;32:1865–71 [PubMed: 21145587]
28. El-Kenawy AEM, Constantin C, Hassan SMA, Mostafa AM, Neves AF, de Araujo TG, et al., 2017 Nanomedicine in Melanoma: Current Trends and Future Perspectives in Ward WH and Farma JM (eds) Cutaneous Melanoma: Etiology and Therapy, Brisbane (AU)
29. Song HB, Wi J-S, Jo DH, Kim JH, Lee S-W, Lee TG, et al., Intraocular application of gold nanodisks optically tuned for optical coherence tomography: inhibitory effect on retinal neovascularization without unbearable toxicity. Nanomedicine: Nanotechnology, Biology and Medicine. 2017;13:1901–1911
30. Schmetterer J. W. K. e. L, Ocular Blood Flow. 2012
31. Remington LA, 2012 Chapter 3 - Uvea Clinical Anatomy and Physiology of the Visual System (Third Edition), Butterworth-Heinemann, Saint Louis pp 40–60
32. Lapierre-Landry M, Gordon AY, Penn JS and Skala MC, In vivo photothermal optical coherence tomography of endogenous and exogenous contrast agents in the eye. Scientific Reports. 2017;7:9228 [PubMed: 28835698]

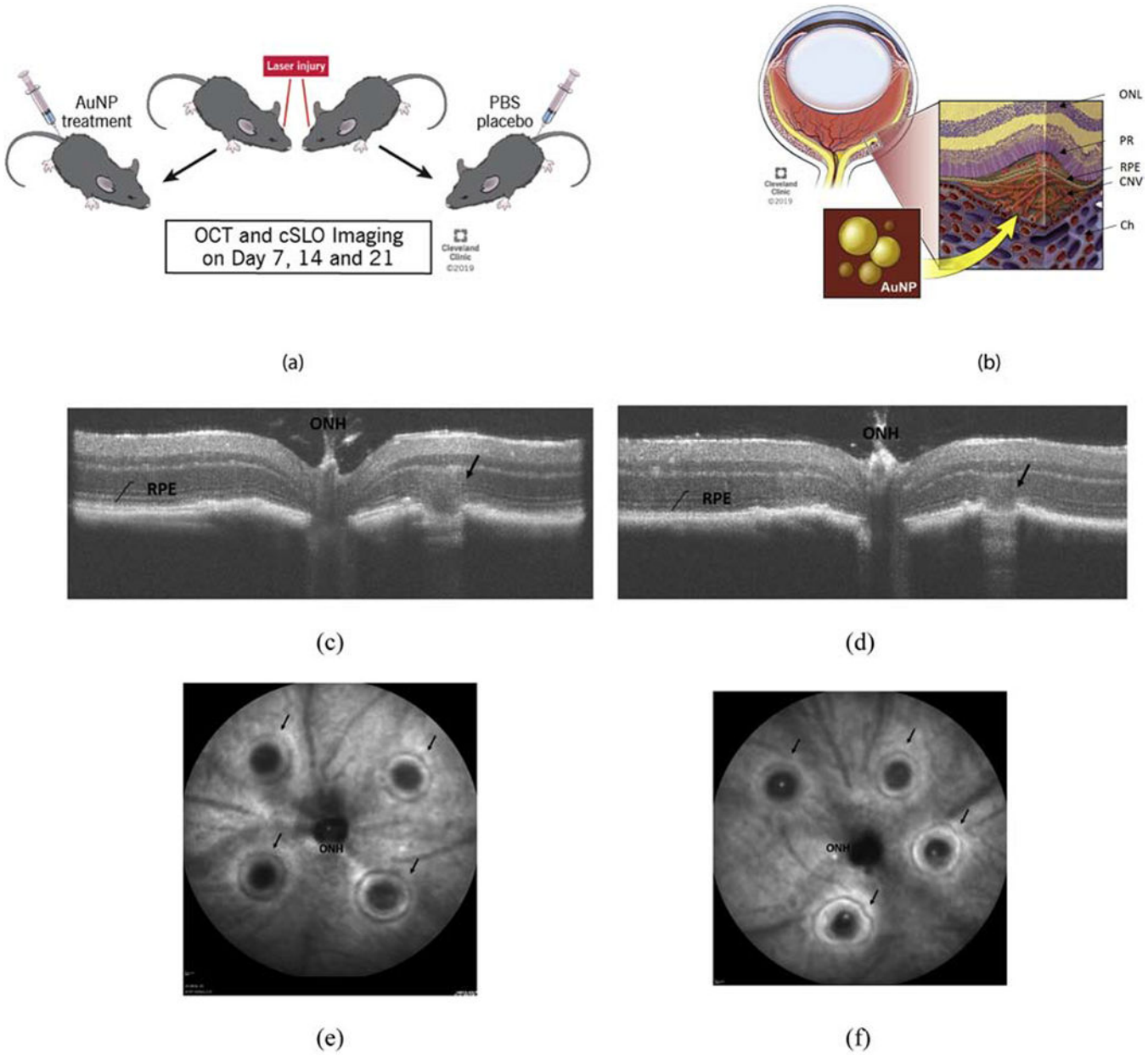

Figure 1:

Experiment design illustration (a) showing the experimental protocol of inducing laser lesion, treatment with intravenously injected AuNP or sham PBS, (b) a schematic of retinal and choroidal layers with a typical CNV lesion, (c) a representative OCT b-scan and cSLO image immediately (Day 0) after the laser injury in control and in (d) treatment mouse, and, a representative image with arrows showing successful laser lesions around the optic nerve head in (e) control and (f) treatment mouse respectively. ONH = optic nerve head, RPE = retinal pigment epithelium, Ch = choriod, PR = photoreceptors, CNV = choroidal neovascularization, and ONL = outer nuclear layer.

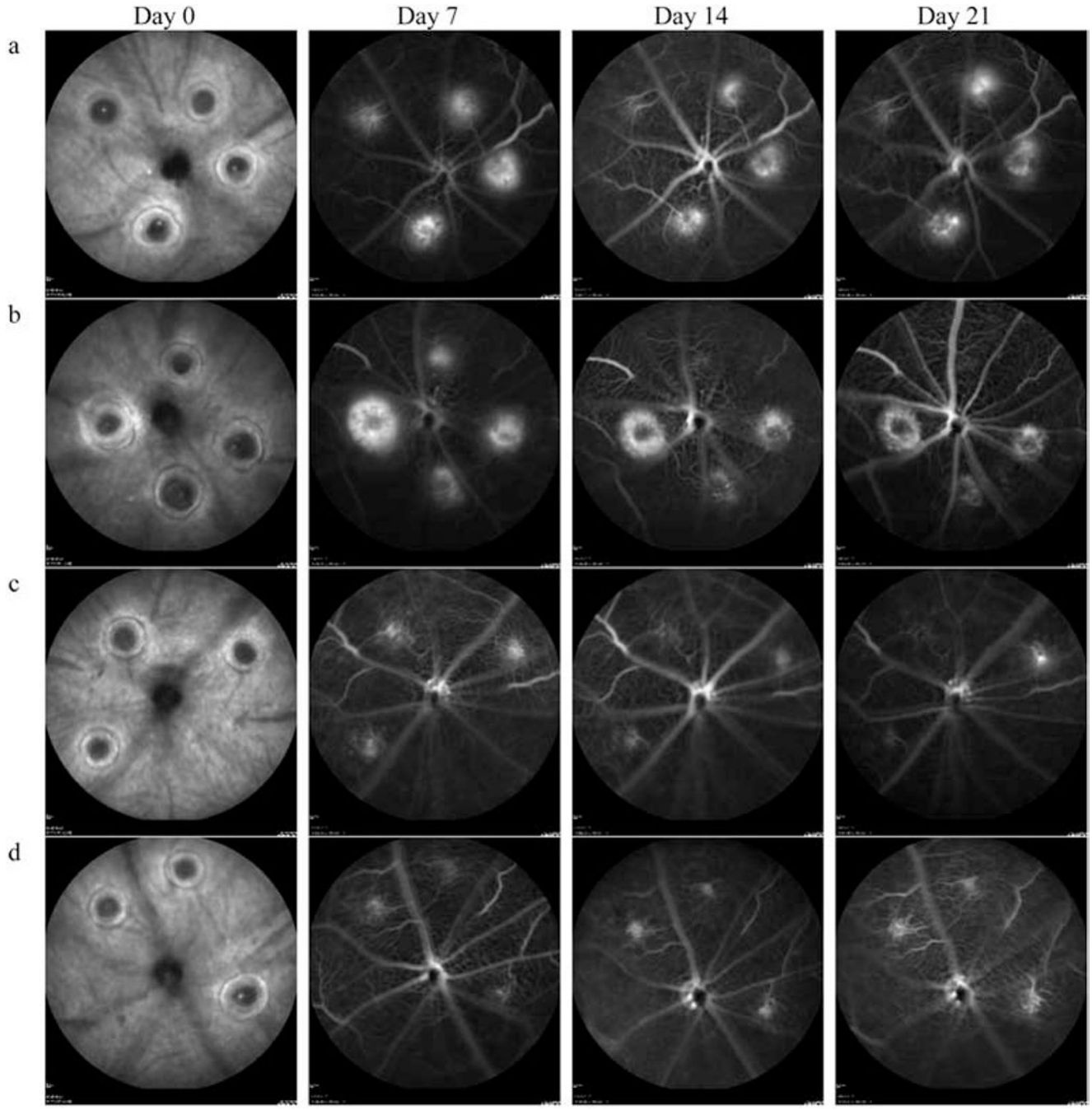

Figure 2:

Fluorescein angiograms of mouse RPE/Choroid interface at day 7, 14, and 21 - post laser injury. Four representative animals are presented: (a) and (b) are sham PBS treated controls and (c) and (d) are AuNP treated. Both the leakage area and intensity of signal are decreased in the treatment group compared to control animals at all three-time points (Day 7. Day 14 and Day 21). Heidelberg Heyex default image processing was used in all the images with normalization and averaging of 25 frames in high-resolution mode. No additional image processing/enhancement was performed.

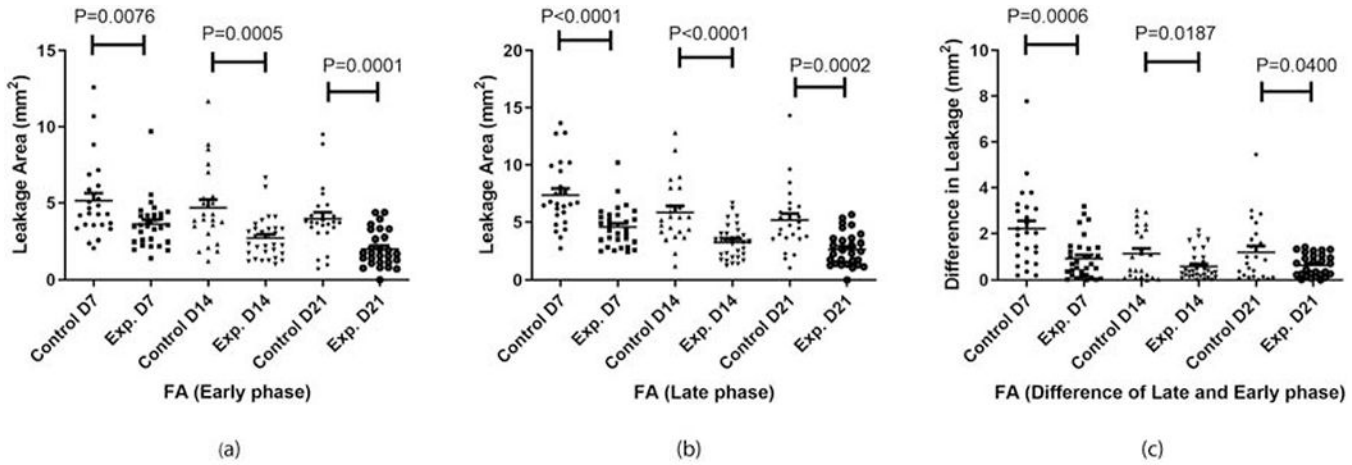

Figure 3:

FA leakage area of controls and experimental group on day 7 (D7), 14 (D14), and 21 (D21) for (a) early phase and (b) late phase fluorescein angiography. Inset (c) represents the difference between the early and late phase leakage area for corresponding groups.

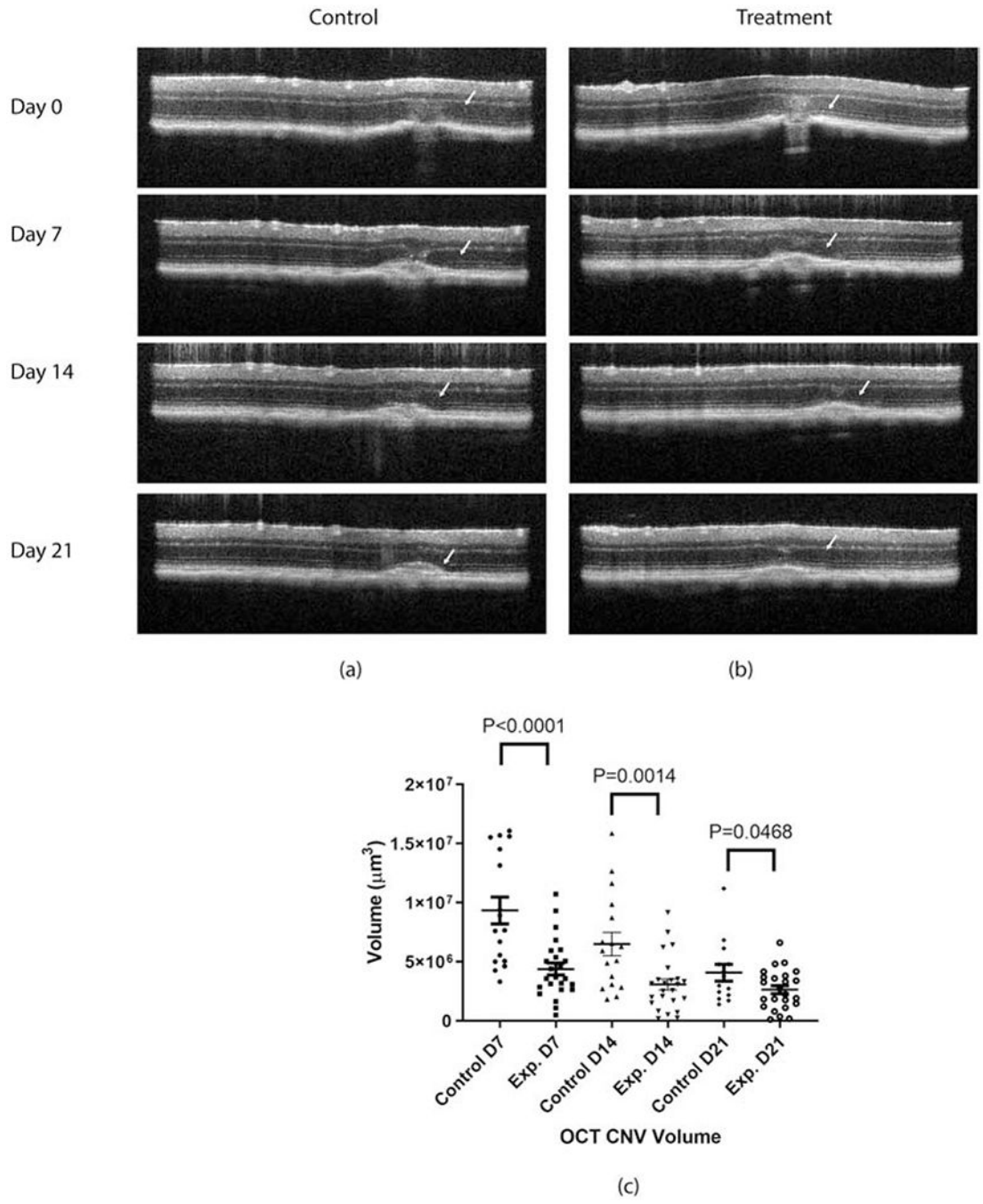

Figure 4:

OCT – CNV volume representative scans of (a) control, (b) experimental mouse on all follow-up time points (i.e. day 7, 14 and 21), and (c) statistical comparison of OCT based CNV volume measured on day 7, 14, and 21 after laser injury. N=17 for controls and n=24 for experimental at each time point.

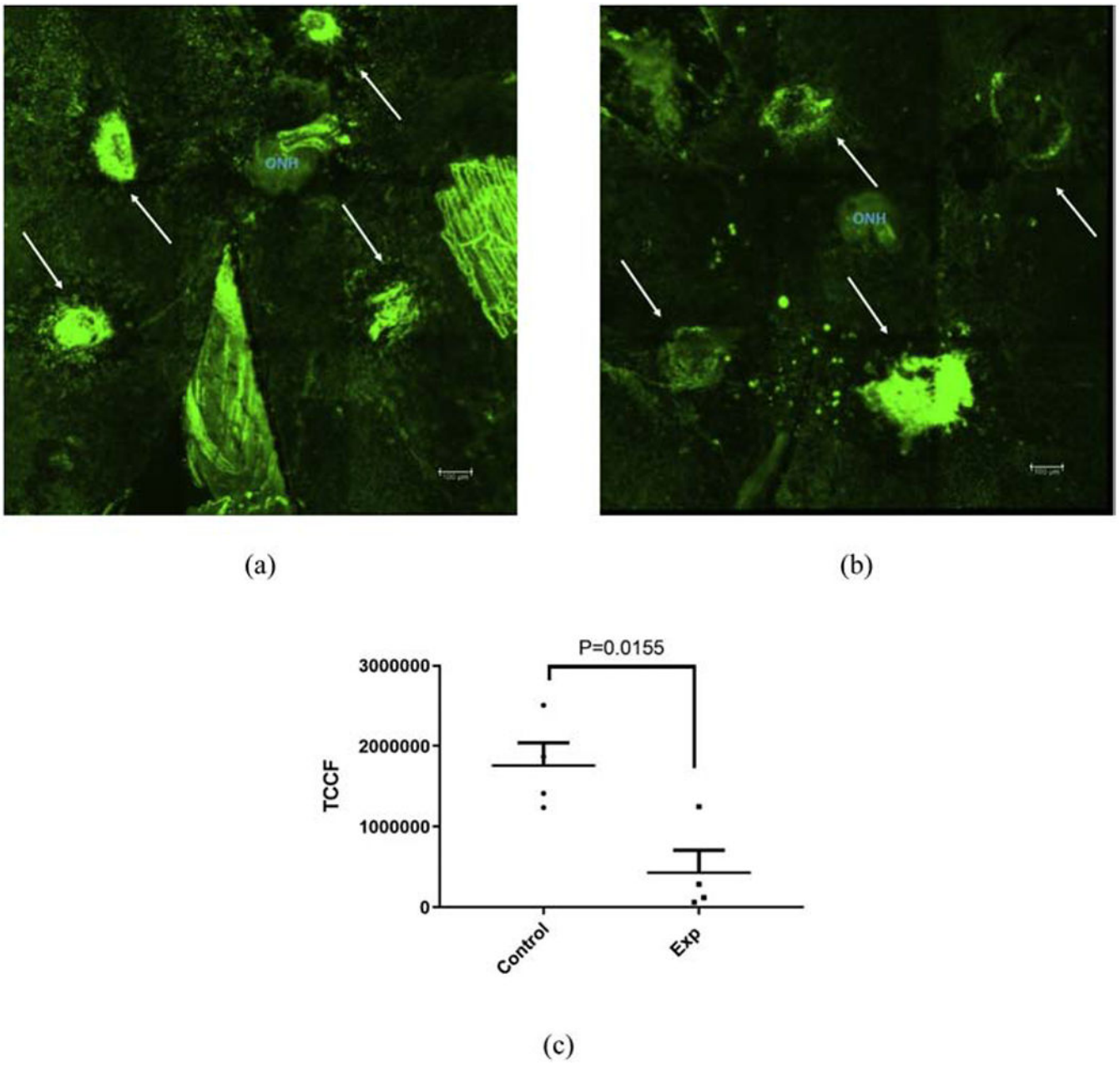

Figure 5:

Choroidal flat mount with Isolectin B4 stained laser induced CNV lesions of a sham treated control mouse retina (a) and AuNP treated experimental mouse retina (b). On average both area and intensity of treated retina (b) appears decreased compared with sham treated (a). Quantification of lesion area with corrected background fluorscence (total corrected cellular fluorescence, TCCF) has been presented in (c) with n=4. Scale bar in (a) and (b) = 100 μm.

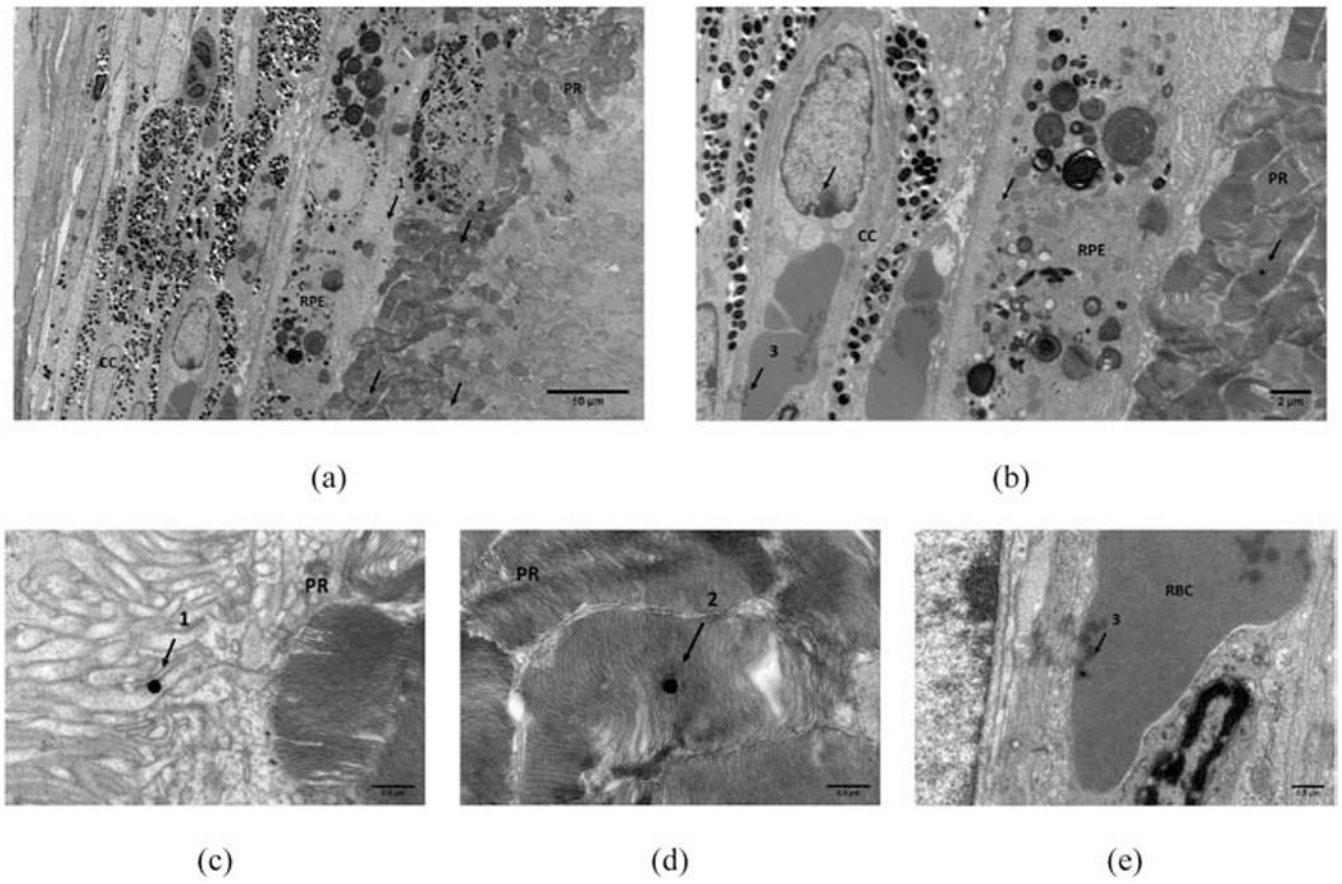

Figure 6:

TEM image of CNV lesion around choroid and RPE-photorecepter showing presence of AuNP (arrows). (a) AuNP present in the PR-RPE and (b) in cc. A high resolution close up of three instances (numbered 1-3 in (a) and(b)) are presented in (c) AuNP's in RPE, (d) in PR, and (e) in RBC of cc. Scale bars used: (a) = 10 um, (b) = 2 um, and (c)-(e) = 0.5 um. RPE = retinal pigment epithelium, cc = choriocapillaris, PR = photoreceptors, RBC = red blood cell.

Table I:

CNV lesion inclusion-exclusion criteria chart for each laser induced lesion in CNV group

Parameter for CNV lesion quality	**Included**	**Excluded**
Visible bubble during laser injury observed using slit lamp	Present	Not-present
Bruch's Membrane rupture observed using OCT	Present	Not-present
Hyperfluorescent central of the lesion observed using *in vivo* infrared imaging of SLO	Present	Not-present
Lesion hit a large retinal blood vessel or lesion looks oddly shaped (non-circular)	Not-present	Present